2022

Using neurophotonic tools to access the effects of repeated blood-brain-barrier opening with focused ultrasound

BOSTON UNIVERSITY

COLLEGE OF ENGINEERING

Thesis

USING NEUROPHOTONIC TOOLS TO ACCESS THE EFFECTS OF REPEATED BLOOD-BRAIN-BARRIER OPENING WITH FOCUSED ULTRASOUND

by

XIAOJIE CHEN

B.S., Shandong University, 2020

Submitted in partial fulfillment of the

requirements for the degree of

Master of Science

2022

Approved by

First Reader

Anna Devor, Ph.D.
Associate Professor of Biomedical Engineering

Second Reader

Xue Han, Ph.D.
Professor of Biomedical Engineering

Third Reader

David A. Boas, Ph.D.
Professor of Biomedical Engineering
Professor of Electrical and Computer Engineering

Acknowledgments

First, I would like to thank my principle investigator, Dr. Anna Devor, for giving me the opportunity to work in her lab, and giving me the chance to work on this project. I would also like to thank all members in Neurovascular Imaging Lab. In particular, I am very grateful to Dr. Martin Thunemann, Dr. Natalie Fomin-Thunemann, Dr. Kıvılcım Kılıç, Patrick Doran, Emily Martin. I would like to thank Dr. Nick Todd, Dr. Cleide Angolano, Dr. Yongzhi Zhang from Brigham and Women's Hospital.

In the end, I would like to thank my mother Lixia Guo, my father Guantong Chen, and my friends Yudian Chen, Yutong Ren, and Yawei Deng, for their endless live, support and encouragement.

USING NEUROPHOTONIC TOOLS TO ACCESS THE EFFECTS OF REPEATED BLOOD-BRAIN-BARRIER OPENING WITH FOCUSED ULTRASOUND

XIAOJIE CHEN

ABSTRACT

The blood-brain barrier (BBB) is a critical protective structure that tightly controls which molecules can pass from the bloodstream into the brain parenchyma. Focused ultrasound (FUS) is an emerging technology that allows the possibility of a non-invasive and controlled opening of the BBB for the delivery of therapeutics that would not otherwise reach the brain. However, the secondary effects of repeated BBB disruption are not fully understood. In this study, we used mesoscopic and microscopic imaging to track neuronal and vascular activity following repeated FUS-BBB opening in mice. We used genetically encoded calcium indicators (GECI) to measure neuronal activity and used reflectance light to estimate changes in oxy-, deoxy- and total hemoglobin levels. The hemodynamic response function was calculated to evaluate the alteration of neurovascular coupling. This study provided a better understanding of the relationship between repeated FUS-BBB opening and the alteration of neurovascular coupling in an animal model.

Contents

List of Figures

List of Abbreviations

BBB	.....	The Blood Brain Barrier
BOLD	.....	Blood Oxygenation Level Dependent
CCD	.....	Charge-Coupled Device
CNS	.....	Central Nervous System
FITC	.....	Fluorescein Isothiocyanate
FUS	.....	Focused Ultrasound
GECI	.....	Genetically Encoded Calcium Indicators
HbO	.....	Oxygenated Hemoglobin
HbR	.....	Deoxygenated Hemoglobin
HbT	.....	Total Hemoglobin
HRF	.....	Hemodynamic Response Function
IgG	.....	Immunoglobulin G
NVC	.....	Neurovascular Coupling
NVU	.....	Neurpvascular Unit
ROI	.....	Region of Interest
sCOMS	.....	scientific Complementary Metal-Oxide-Semiconductor
SNR	.....	Signal to Noise Ratio
TB	.....	Trypan Blue

Chapter 1

Introduction

The blood brain barrier (BBB) is a critical structure that tightly regulates the movement of ions, molecules, and cells between the bloodstream and the brain, mainly composed of endothelial cells and pericyte cells. Endothelial cells are held together by tight junctions, which create a high-resistance paracellular barrier to molecules and ions (Daneman et al., 2015). The BBB is a highly selective semipermeable border. It can prevent solutes in the circulating blood from non-selectively crossing into the extracellular fluid of the central nervous system (CNS) where neurons reside. Because the BBB maintains the ionic balance, it has raised difficulty in targeting drugs to the brain, which involves going through the BBB (Gross et al., 1990). Different ways have been tried to deliver therapeutics to the brain, such as osmotic and chemical disruption of the BBB, which are all limited by invasiveness, poor spatial distribution, or low efficacy (Hersh et al., 2016).

In the past few years, animal studies have demonstrated that low-power ultrasound pulses combined with microbubbles can temporarily disrupt the BBB with negligible associated effects on the brain (Hynynen et al., 2001). This phenomenon can be used as a noninvasive method for targeted drug delivery in the CNS. Combining the ultrasound pressure field and gas-filled microbubbles circulating in the vasculature, one could potentially disrupt the tight junction in purpose (Todd et al., 2020). It could facilitate the use of therapeutic agents that are currently stopped by the BBB, such as chemotherapy agents or drugs designed to treat neurodegenerative diseases

(Aryal et al., 2014; Meairs, 2015).

Besides disrupting the BBB, several secondary effects have been observed following the application of the FUS-BBB opening, including a generalized inflammatory response (McMahon et al., 2017; Kovacs et al., 2018), reduction of amyloid β plaques and hyperphosphorylated tau proteins (Raymond et al., 2008; Jordao et al., 2010), changes in brain transcriptome and proteome profiles (McMahon et al., 2017), and alteration of cerebral blood flow (Raymond et al., 2007). All the secondary effects mentioned may result in the suppression of neuronal activity.

The brain receives energy through the blood supply, and neuronal activity imposes dynamic and regionally diverse energy requirements (Iadecola, 2017). It has been shown that neuronal activity is closely related to cerebral blood flow (Kleinfield et al., 2011). This is termed 'neurovascular coupling (NVC)'. NVC describes the complex mechanism of communication between neurons, astrocyte glial cells, and cerebral vessel cells, which form the neurovascular unit (NVU) (Lecrux et al., 2011). This term describes that if there is neuronal activity, it can lead to blood vessels dilation or constriction, which thereby changes blood flow and the changes in the total concentration of hemoglobin, and the ratio of oxygenated to deoxygenated hemoglobin (Valley et al., 2020; Allen et al., 2017; Wekselblatt et al., 2016). In a healthy brain, cerebral blood flow and oxygen delivery rapidly increase at activated brain sites (Kisler et al., 2017) to satisfy the demand for energy and nutrients. Injuries, diseases, and clinical treatments may disrupt the neurovascular coupling, leading to brain damage. Increasing evidence indicates that the impact of FUS-BBB opening treatment reaches all cell types in the NVU (Chatterjee et al., 2014; Kovacs et al., 2016; Todd et al., 2020). Todd et al. have shown a significant decrease in hind paw stimulation induced blood-oxygen-level-dependent (BOLD) response in the somatosensory cortex of rats targeted for FUS-BBB opening, which also indicates a change in NVC (Todd et al.,

2020).

Capturing images of mice brains, we got the chance to quantitatively investigate neurovascular coupling. Mesoscopic fluorescence calcium imaging has been widely used to monitor neuronal activity in vivo (Ma et al., 2015). And a common method to estimate hemodynamics during a fluorescence measurement is to simultaneously record diffuse reflectance measurements benefitting from the different absorption coefficients of oxy-hemoglobin and deoxy-hemoglobin to the same light (Ma et al., 2015). In this thesis, we measured the hemodynamics signal and calcium signal simultaneously and studied the relationship between neuronal and hemodynamic activity. By assuming that the hemodynamic response function (HRF) is the kernel convolved to the neuronal activity, we used the deconvolution method to estimate the HRF and compared it before and after repeated FUS-BBB openings. Moreover, benefitting from the single artery resolution, two-photon imaging was also used in this study to observe the vessel leakage and alteration of neurovascular coupling.

Chapter 2

Results

2.1 The blood brain barrier opening occurred after focused ultrasound treatments.

In a healthy brain, the blood brain barrier provides a stable environment for neural cells (Abbott et al., 2009). The tight junction between endothelial cells excludes 98% of small molecules, including molecules that have molecular weight under 400Da, and 100% of large molecules (molecular weight greater than 500Da) (Pardridge et al., 2005). Benefiting from the cavitation effects from the circulating microbubbles interacting with focused ultrasound sonication (Wu et al., 2020), focused ultrasound combined with microbubbles (Optison) has shown a potential to disrupt blood brain barrier temporarily in a non-invasive manner (Hynynen et al., 2001) and enhance the permeability of the targeted vessel (Park et al., 2010; Tsai et al., 2013). As a result, molecules that do not usually travel the blood brain barrier can cross from the bloodstream to the neighboring tissues. For example, the bllod brain barrier usually rejects immunoglobulin G (IgG) because of its large molecular weight (150KDa). Experimental evidence shows that IgG can enter the parenchyma after the FUS-BBB opening (Sheikov et al., 2004; Raymond et al., 2008). To verify that the blood brain barrier opening has occurred in our experiments, we performed IgG staining on the brain slices. The samples were collected from mice that were sacrificed at different time points (1h, 6h, 12h, 24h) in the presence or absence of FUS-BBB opening treatments (Figure. 1). In the experiment group, IgG staining appeared in the so-

matosensory cortex, which received FUS-BBB opening treatment. This indicated that the blood brain barrier opening occurred after focused ultrasound treatment. We also observed the extravasation of Trypan Blue (67KDa when bound to albumin) after focused ultrasound treatments from the brain slices collected from mice that were sacrificed at different time points (1h, 12h) after FUS-BBB opening treatments (**Figure. 2.1**). Combining the results from IgG staining and TB autofluorescence, our focused ultrasound treatments have increased the permeability of the blood brain barrier.

In addition to *in vitro* verification, we also evaluated the effect of focused ultrasound treatment with *in vivo* imaging. We intravenously injected FITC dextran through the mouse tail vein immediately after the focused ultrasound treatments. FITC fluorescence was observed in parenchyma by our two-photon imaging setup (**Figure. 2.2**).Both **Figure. 2.2A** and **Figure. 2.2B** were acquired in mice brains at 40mins after the focused ultrasound treatments

Both *in vitro* and *in vivo* experiments have confirmed that the blood brain barrier opening happened after the focused ultrasound treatments.

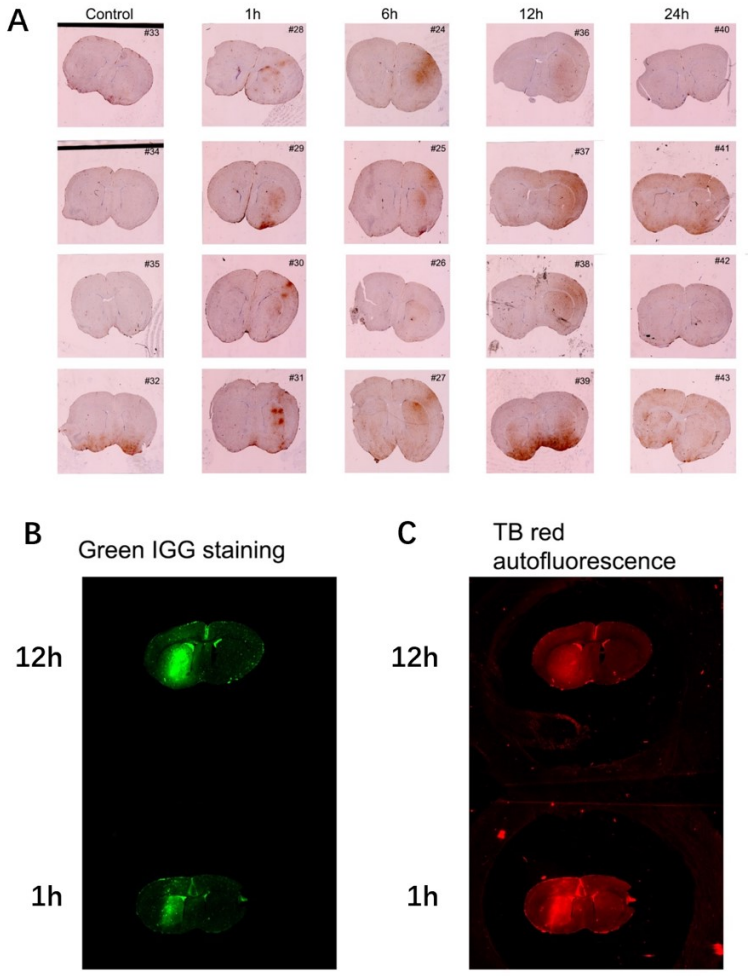

Figure 2·1: **A**: IgG immunostaining detected by light microscopy. We collected mice brains from mice sacrificed at different time points (1h, 6h, 12h, 24h) in the presence or absence of focused ultrasound treatments. Most mice brains in the control group didn't show IgG staining, while the staining appeared in the somatosensory cortex collected after the treatments. **B**: IgG antibody (conjugated to an infrared dye) autofluorescence appeared in the somatosensory cortex. The sample was collected at 1h and 12h after the focused treatments. **C**: Trypan Blue autofluorescence appeared in the brain regions that received focused ultrasound treatments. The sample was collected at 1h and 12h after the focused treatments.

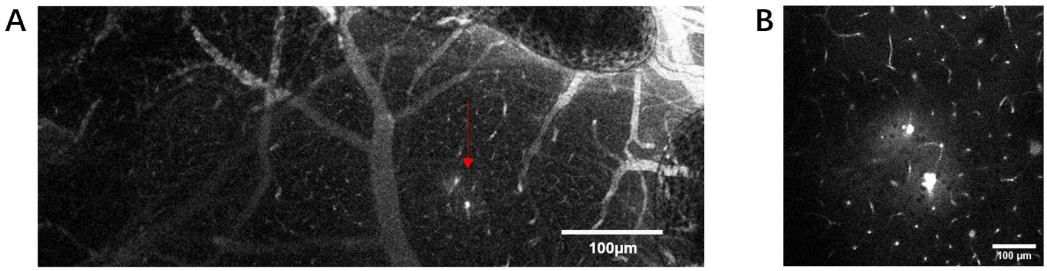

Figure 2·2: Vessel leakage measurements on mouse Thy1-45 after focused ultrasound treatment. Two-photon images were acquired after 40mins of treatment and injection of FITC dextran dye. **A**: The region pointed by the red arrow became brighter over time, indicating the increasing FITC dextran leakage due to the focused ultrasound treatments. **B**: Vessels appeared as 'blobs', and FITC dextran leaked out from the vessel to the neighbor tissues (the bright region).

2.2 The cranial glass window does transit the focused ultrasoun pulse.

The cranial glass windows were implanted into mice brains for the imaging procedures following the focused ultrasound treatments. To evaluate whether the cranial glass window prevented the focused ultrasound wave, we performed hydrophone measurements. The result showed 10% attenuation of FUS intensity due to the glass coverslip. Therefore, for our future experiments, we will increase the input voltage by 10% to the transducer, which has a linear relationship with the input pressure. The trypan blue dots on the area receiving focused ultrasound treatments showed that the blood brain barrier was opened to an identical degree **(Figure. 2.3)** in brains collected from mice with and without cranial glass windows. The cranial glass window does not prevent the FUS-BBB opening in a significant way.

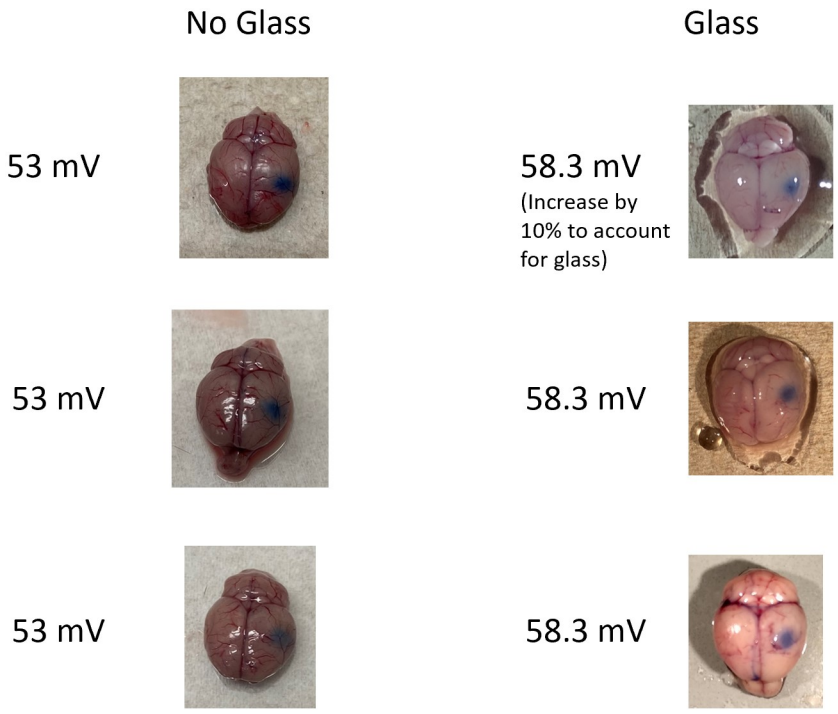

Figure 2·3: Trypan blue staining. The blue dots on the brains show the blood brain barrier opening in the somatosensory cortex receiving focused ultrasound treatments. The brains were collected from mice with and without cranial glass windows.

2.3 The focused ultrasound treatment protocol we used introduced negligible alteration of neurovascular coupling.

Neurovascular coupling has been broadly studied as the mechanism that links transient neuronal activity to the subsequent change in cerebral blood flow (Hendrix et al., 2019). The brain does not possess any reserve of energy or oxygen, and thus relies on constant perfusion to fulfill its energetic demands, particularly during increased neuronal activity (Siesjo 1971). Therefore, neuronal activity is usually followed by blood vessel dilation and the alteration of the concentration of different types of hemoglobin. At the microscopic level, the neurovascular unit is comprised of the cerebral vessel

cells, the neuron, and the astrocyte glial cells. Signal molecules such as glutamate and potassium are released by the astrocytes upon the neuronal activity, playing an important role in the complex balance of vasodilation and vasoconstriction (Metea et al., 2006).

Recent studies have convinced that FUS-BBB opening treatment can induce astrocyte reactivity and microglia activation as a result of a sterile inflammatory response in healthy mice (Chatterjee et al., 2014; Kovacs et al., 2016). An average reduction in vessel diameter of approximately 50% following the focused ultrasound treatments was also discovered as evidence of disruption of neurovascular coupling (Raymond et al., 2007).

To evaluate the alteration of neurovascular coupling introduced by focused ultrasound treatments, we measured intrinsic hemodynamic signal and calcium signal in mice responding to sensory stimulation using mesoscopic imaging. Air puff stimulation on mice whiskers was used to evoke hemodynamic and neuronal responses. We stimulated mice 12 times following a 10-second baseline. Each stimulation was performed at 3Hz for 2 seconds. The interval between each stimulation was 30 seconds. The stimulation run was repeated twice. We applied mesoscopic imaging on mice brains one day before and one day after the focused ultrasound treatments in all treatment weeks. On the treatment day, imaging was also performed right after the treatment.

After acquiring wild field images, we extracted hemodynamic and neuronal response traces. We averaged the signal through different stimulation trials (12 trials in one measurement) to reduce the noise (**Figure. 2.4)**. In the results derived from mouse Thy1-45 and Thy1-46, there is no significant alteration in the shapes of the curves corresponding to the hemodynamic and neuronal response signals. All suppressions and enhancements on the hemodynamic signals were accompanied by the

calcium signal alteration.

To evaluate the change in hemodynamic and neuronal activities, we performed dimensional reduction on our data sets. We condensed the shape information over the multiple values into one number. We chose the amplitude of response peak as parameters to estimate the alteration of hemodynamic and neuronal activities responding to air puff stimulation, since the amplitude of peak had a high signal to noise ratio (SNR) in our data sets. All data points were plotted in **Figure. 2.5**. Three colors marked data points from three groups, including the data collected before the treatments, on the treatment day, and after the treatments. The variability of data points was due to unavoidable factors, such as mouse brain dynamic state, measurements noise, and differences in the position of stimulus across experimental sessions. To evaluate the alteration of neurovascular coupling introduced by the focused ultrasound treatments, we also plotted the central points and the linear relationship between the amplitude of neuronal and hemodynamic response peaks of three groups. In the results of mouse Thy1-45, differences between the data collected before the treatments, on the treatment day, and after the treatments were negligible. This result indicated that the neurovascular coupling remained after the focused ultrasound treatments. In the results of mouse Thy1-46, the central point located differently compared with the central points in other two groups, indicating that the neurovascular coupling was disrupted. However, the similarity between the data collected before and after the treatments showed that neurovascular coupling recovered after the focused ultrasound treatments. In addition, the allergic reaction to human albumin in the microbubbles (Optison) might also introduce neurovascular uncoupling. Combining the results of mouse Thy1-45 and mouse Thy1-46, the strong coupling between the hemodynamic and neuronal activities remained in the brain and had not been significantly disrupted by the repeated focused ultrasound treatments.

To assess the alteration of neurovascular coupling in a more accurate way, we calculated the hemodynamic response function (HRF), which represents the transfer function linking neuronal activity with the hemodynamic signal (Rangaprakash et al., 2022). The hemodynamic signal can be thought of as the convolution of neuronal activity with HRF. Therefore, a least-square deconvolution method (Ma et al., 2016) was applied pixel by pixel to estimate the HRF. We averaged the HRFs corresponding to the brain region and summarized all spatially averaged HRF traces in **Figure. 2.6**. Negligible alteration happened in the shape of HRFs. There was no clear pattern proving that the focused ultrasound treatments disrupted the neurovascular coupling significantly.

We tested the deviation in neurovascular coupling by testing how well the pre-treatment HRF could be used to predict the post-treatment hemodynamic response. We took the HRF from pre-treatment (first-day measurement) data to predict the HbT signal for the following days. Correlation coefficients were calculated between the predicted and measured HbT signals **(Figure. 2.7)**. In the first treatment week, both mouse Thy1-45 and mouse Thy1-46 lost correlation on the treatment day, and recovered after. No clear pattern was observed for the rest days. The mice's allergic reaction to the microbubbles (Optison) we used in this study might also cause the suppression of neuronal activity and neurovascular uncoupling, and disturb the results we have shown above. We chose another microbubble agent (Definity) for further experiments. The ability of Definity to facilitate focused ultrasound treatments opening the blood brain barrier has been tested with Trypan Blue autofluorescence **(Figure. 2.8)**. More details will be discussed in the following session.

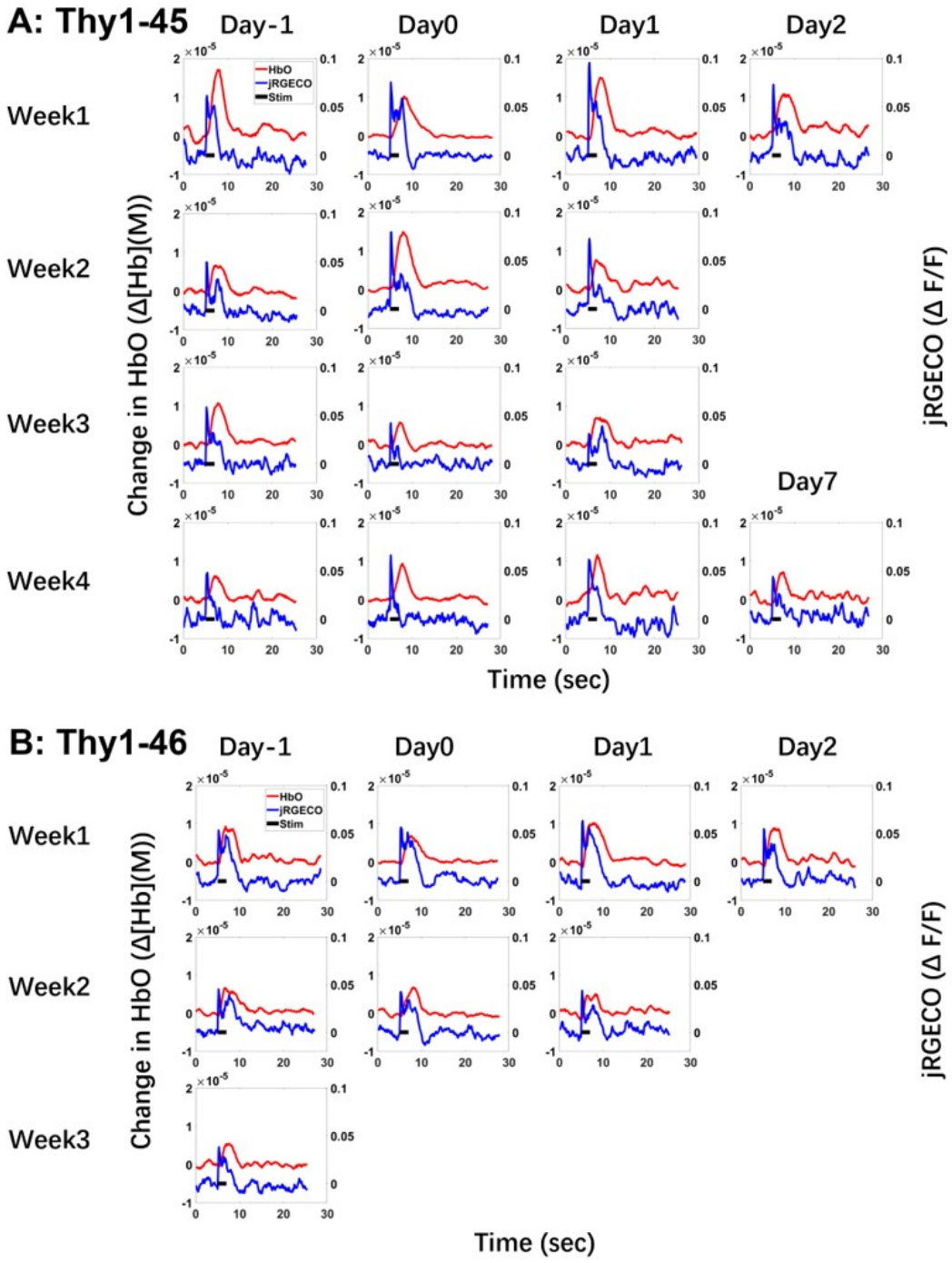

Figure 2·4: **A**: The trial-averaged time course of hemodynamic and neuronal responses to 12-trial air puff stimulation for mouse Thy1-45. **B**: The trial-averaged time course of hemodynamic and neuronal responses to 12-trial air puff stimulation for mouse Thy1-46. Mouse Thy1-46 died on the third treatment day.

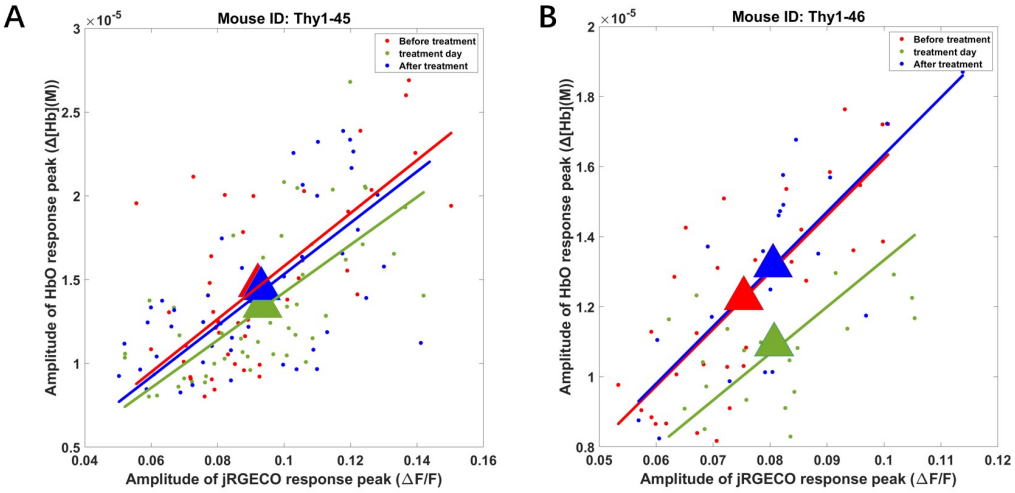

Figure 2·5: Neurovascular coupling remained after the focused ultrasound treatments. Three colors mark data points in three clusters. Red, green and blue represent the data points collected before the treatments, on the treatment days, and after the treatments, respectively. Filled triangles are the central points for the data points in each cluster. Lines represent the linear relationships between the amplitude of neuronal and hemodynamic response peaks.

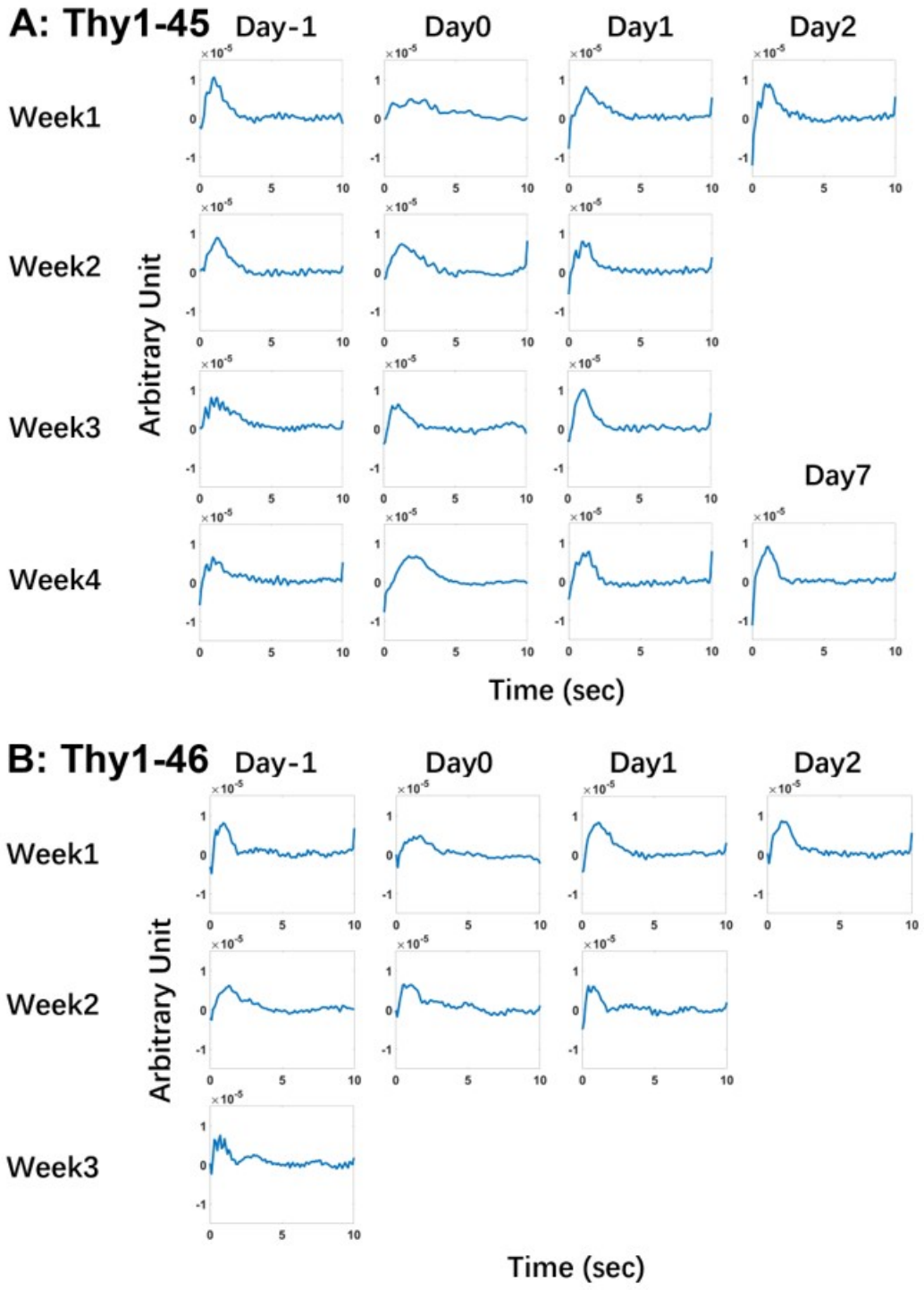

Figure 2·6: The HRFs of mouse Thy1-45 and mouse Thy1-46, respectively.

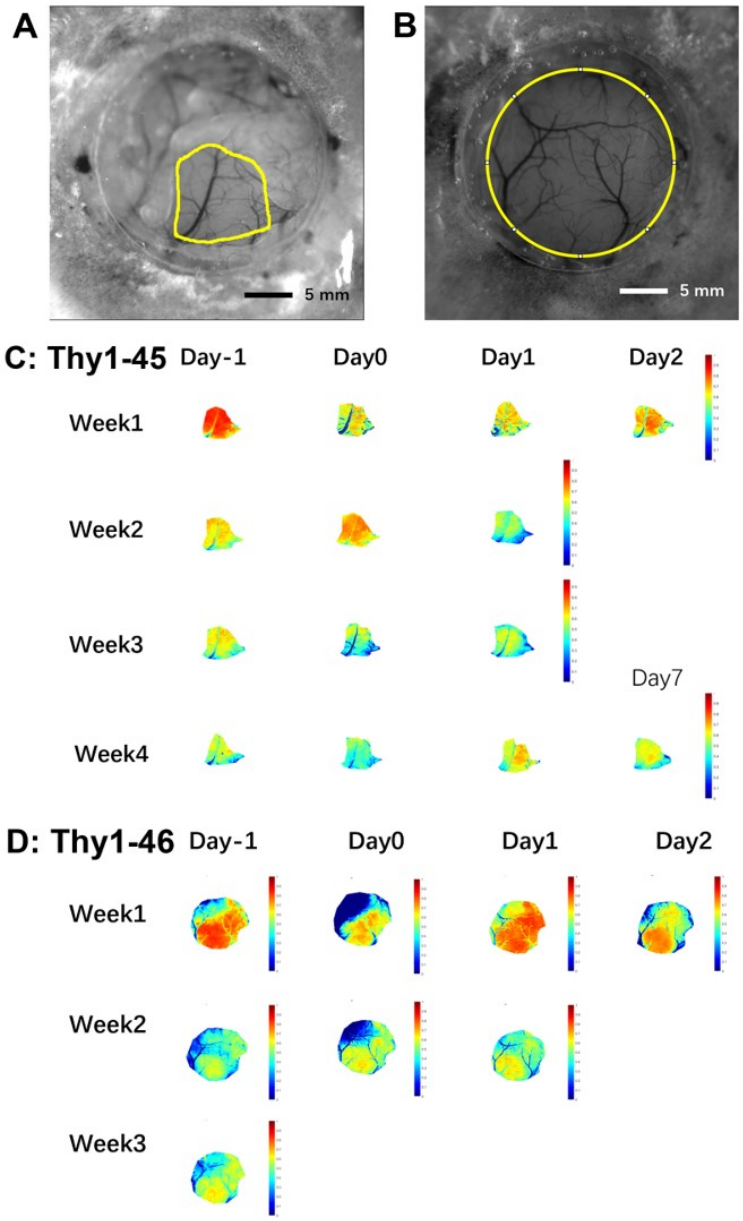

Figure 2·7: We took the brain region without the bone regrowth as our region of interest (ROI). Figures were acquired under the illumination of 525nm LED. **A**: The ROI for mouse Thy1-45. **B**: The ROI for mouse Thy1-46. **C, D** Correlation coefficients maps for mouse Thy1-45 and mouse Thy1-46, respectively. The correlation coefficients were calculated between the predicted and measured HbT signals. The predicted HbT signals were predicted by convolving the HRF from the first day and the measured neuronal signals.

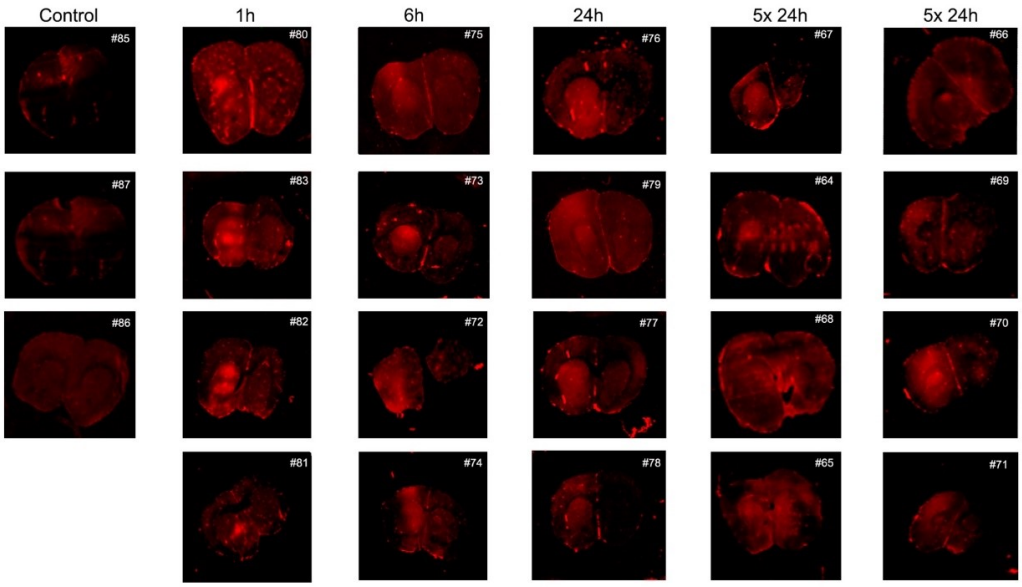

Figure 2·8: Trypan blue autofluorescence appeared in the brain regions that received focused ultrasound treatments. The samples were collected from mice sacrificed at different time points (1h, 6h, 12h, 24h, 5*24h) in the presence or absence of focused ultrasound treatments.

2.4 Space-invariant HRF can be applied to small brain regions.

To test the accuracy of our deconvolution model, we convolved the spatially averaged neuronal signal with the spatially averaged HRF to predict the hemodynamic signal. Both neuronal signal and HRF were extracted from the same day. **Figure. 2.9** is an example showing that the predicted signal was a good fit for the measured signal. Besides, pixelated correlation coefficients between the predicted and measured hemodynamic signal were also calculated **(Figure. 2.10)**. We convolved the HRF averaged from the brain region with the neuronal signal extracted from the same day pixel by pixel. Because of bone regrowth, the ROI of mouse Thy1-45 was a small region (1x1mm3). The high correlation coefficients indicated homogeneous neurovascular coupling in the small region, given that the HRF was space-invariant.

The ROI of mouse Thy1-46 was almost the whole exposed window (5x5mm3). At the identical region as the ROI of mouse Thy1-45, the correlation coefficients were also high. A clear drop in correlation coefficients was observed in other regions. Applying space-invariant HRF revealed inhomogeneity on a larger scale.

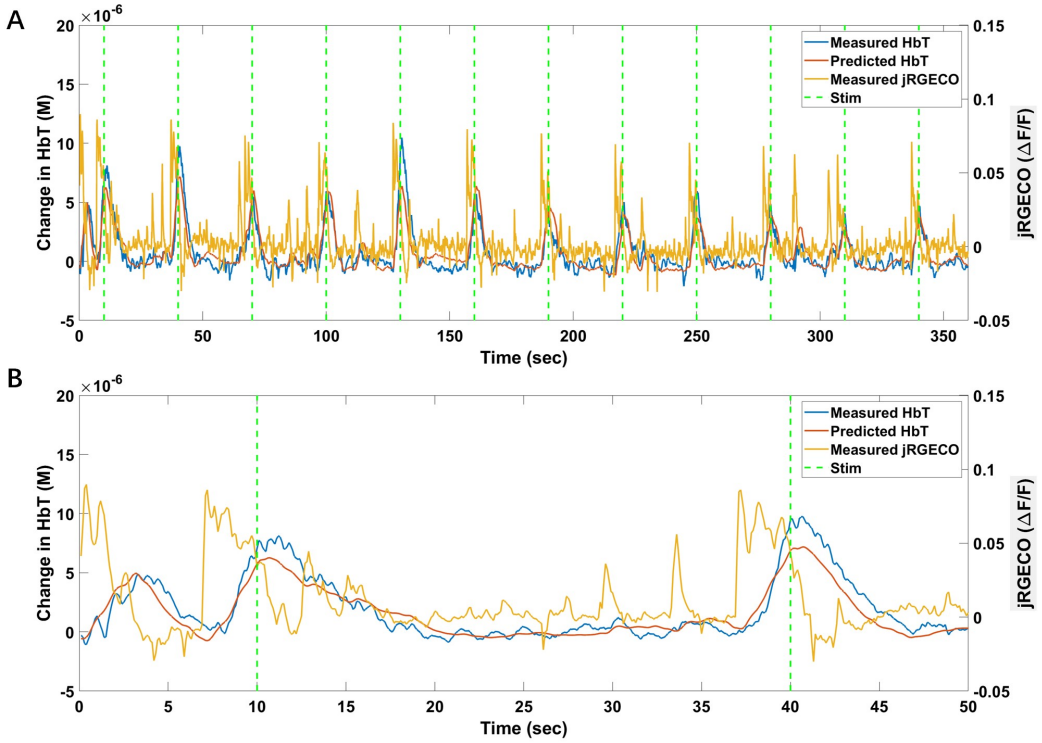

Figure 2·9: Our deconvolution model was a good fit.

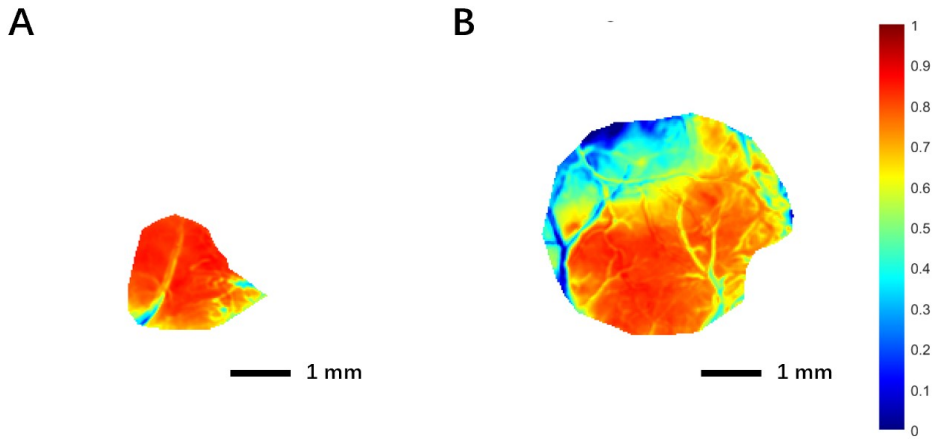

Figure 2·10: Correlation coefficient maps for mouse Thy1-45 and Thy1-46, respectively. Correlation coefficients were calculated between the measured hemodynamic signals and predicted hemodynamic signals. The predicted hemodynamic signal was calculated by convolving the space-invariant HRF and pixelated neuronal signals.

Chapter 3

Methods

3.1 Animal preparation and experimental design

Male and female Thy1-jRGECO1a mice (Jackson labs, STOCK Tg(Thy1-jRGECO1a) GP8.20Dkim/J) were used in this experiment. Two Wild type mice were also used to provide more information about the hemodynamic response. On the surgery day, mice skulls on mice's somatosensory cortexes were removed. Custom-made titanium head posts were fixed to mice skulls for the following experiments, and 5-mm round coverslips were used to cover the exposure on mice skulls. After surgery, mice were allowed to recover for four weeks. During the last two weeks of recovery, mice underwent training procedures in a custom imaging cradle to adapt to the imaging setup and environment.

Two-photon baseline imaging was performed a week before the first FUS-BBB opening treatment, measuring the neuronal activity and vessel dilation responding to sensory stimulation. After pre-treatment measurement, FUS-BBB opening treatments were repeated once a week, four weeks in total. Each FUS treatment was given after the intravenous injection of 0.1 mL/kg Optison microbubble ultrasound contrast agent under anesthesia with 2% isoflurane in medical air. The ultrasound beam (690 kHz, 10-ms bursts applied for 120 s at a frequency of 1 Hz) was focused on the somatosensory cortex of mice using a pressure of 0.32 MPa. In treatment week, we performed mesoscopic imaging one day before FUS-BBB opening treatment and one day after. On the day that mice received FUS-BBB opening treatment, mesoscopic

imaging was performed right after the treatment. After the first and third treatments, we observed vessel leakage using two-photon microscopy. One week after the fourth treatment, we measured neuronal activity and vessel dilation responding to sensory stimulation again with two-photon microscopy.

3.2 IgG immunostaining and Trypan Blue autofluorescence

To evaluate the effects of focused ultrasound treatments on the BBB opening, we performed Trypan Blue detection and IgG staining assays. The protocol is detailed elsewhere (Nicholas et al., 2002). Briefly, we injected Trypan Blue through the mouse tail vein following the focused ultrasound treatments. Then we collected the brains from mice sacrificed at different time points (1h, 6h, 12h, 24h). Subsequently, we cut the brain regions that had blue dots into 3mm slices. Non-treatment animals were also used in control. The brain slices were then fixed with buffered formalin 10% for 24-48h, followed by dehydration and paraffin embedding. The collected samples were cut (6m) with Microtome. We used Li-Cor brochure system to observe the Trypan Blue autofluorescence at 680nm.

We baked the other samples for 15mins at 56°C to melt the paraffin. The paraffin was removed by incubating with zyline for 6mins twice. Following the rehydration with 95% ethanol and 75% ethanol for 1min, respectively, the samples were washed with filtered water for 2mins twice. Subsequently, the samples were blocked with 7% horse serum in PBS for 30mins. We incubated the samples with biotinylated rabbit anti-mouse IgG antibodies, combined with streptavidin-HRP in the ABC (Avidin Biotin Complex) method and DAB chromogenic detection system. We detected the samples with light microscopy. In parallel, we also incubated several pieces of samples with the antibody conjugated to infrared dye. And we used Li-Cor brochure system to detect the autofluorescence.

3.3 Mesoscopic imaging setup

Mesoscopic imaging was performed to simultaneously measure hemodynamic and neuronal activities after FUS BBB opening treatments. The head of the mouse was illuminated with 525nm, 590nm, and 625nm LED light sources (Chrolis, Thorlab), where the 590nm channel was used to excite jRGECO (565/24nm filter was added to the 590nm channel in Chrolis LED source), and the reflectance signal in the 525nm and 625nm channels were used to calculate the hemoglobin concentration variation. The 525 nm wavelength is a high-contrast isosbestic point of the hemoglobin absorption spectra, meaning that both HbO (orange dotted line in **Figure. 3.1**) and HbR (blue dotted line in **Figure. 3.1**) have the same absorption coefficient values to 525nm light, making the measurement independent of oxygenation and sensitive only to changes in HbT. Conversely, 625 nm light is sensitive primarily to HbR, with a much lower absorption overall compared with 525 nm (Ma et al., 2015). Therefore, the reflectance lights of 525nm and 625nm light indicate the amount of light that was absorbed by different hemoglobin species while scattering in the tissue. In experiments, we controlled the intensity of 525nm light to reduce the excitation of jRGECO.

For every imaging session, we performed two baseline measurements (6min) and two sensory-evoked measurements with air puff stimulations on mouse whiskers. In each sensory-evoked measurement, we stimulated the mouse 12 times (trials) with 30 seconds intervals at 3Hz for 2s following 10 seconds baseline. The stimulation run was repeated twice. A custom MATLAB code was used to control LED, air puff, and trigger the camera. Water was added to the surface of the cranial window to avoid that one part of the brain is out-of-focus due to the brain curvature. The exposure time (12.5ms) for every frame was set inside the camera software. Because of the limited intensity of 565nm jRGECO excitation wavelength due to the filter, we

shined the 565nm wavelength light to the mouse brain three times and acquired three images for calcium signal in one imaging cycle to improve the SNR **(Figure. 3.2)**.

During the imaging, a CCD camera (Basler) was used to monitor mouse behavior and pupil **(Figure.3.3)**. We used an infrared 940nm LED light source to illuminate the mouse face to be able to observe mouse face in the dark, which cannot be detected by the mouse eye and has no effect on them. We used a scientific complementary metal-oxide-semiconductor (sCMOS) camera (Sona, Andor) to capture brain images. We used a 523/610nm dual-band bandpass filter from Semrock (523/610 nm BrightLine®; FF01-523/610) to transmit light from 525nm and 625nm channel, and the jRGECO emission light, but to block everything else. 900nm short pass filter was also used to block the light from the LED source to the Sona camera. The mesoscopic imaging process diagram is shown in **Figure. 3.4**.

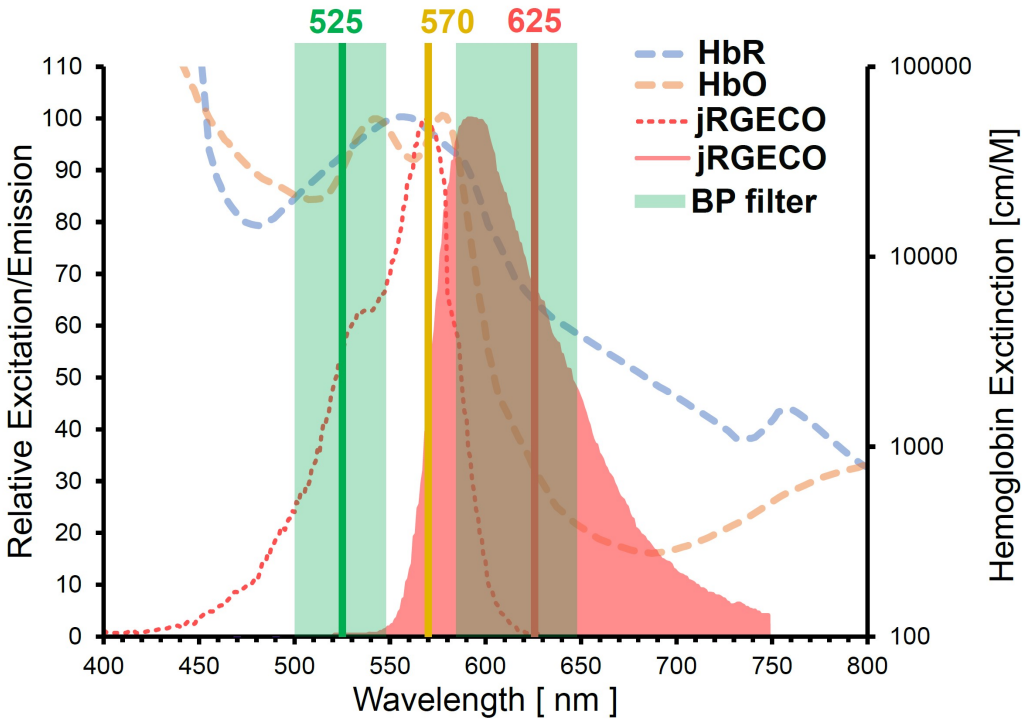

Figure 3·1: The absorption spectra of oxy- and deoxyhemoglobin (HbO and HbR), and the excitation and emission spectra for jRGECO. The three solid lines representing 525nm, 570nm, and 625nm are the wavelengths we used in this study. The green shadings show the spectra for 523/610 bandpass filter. All the wavelengths that we need to collect (reflectance from 525nm and 625nm channels, and the jRGECO emission light) can go through this bandpass filter, while the jRGECO excitation light was blocked.

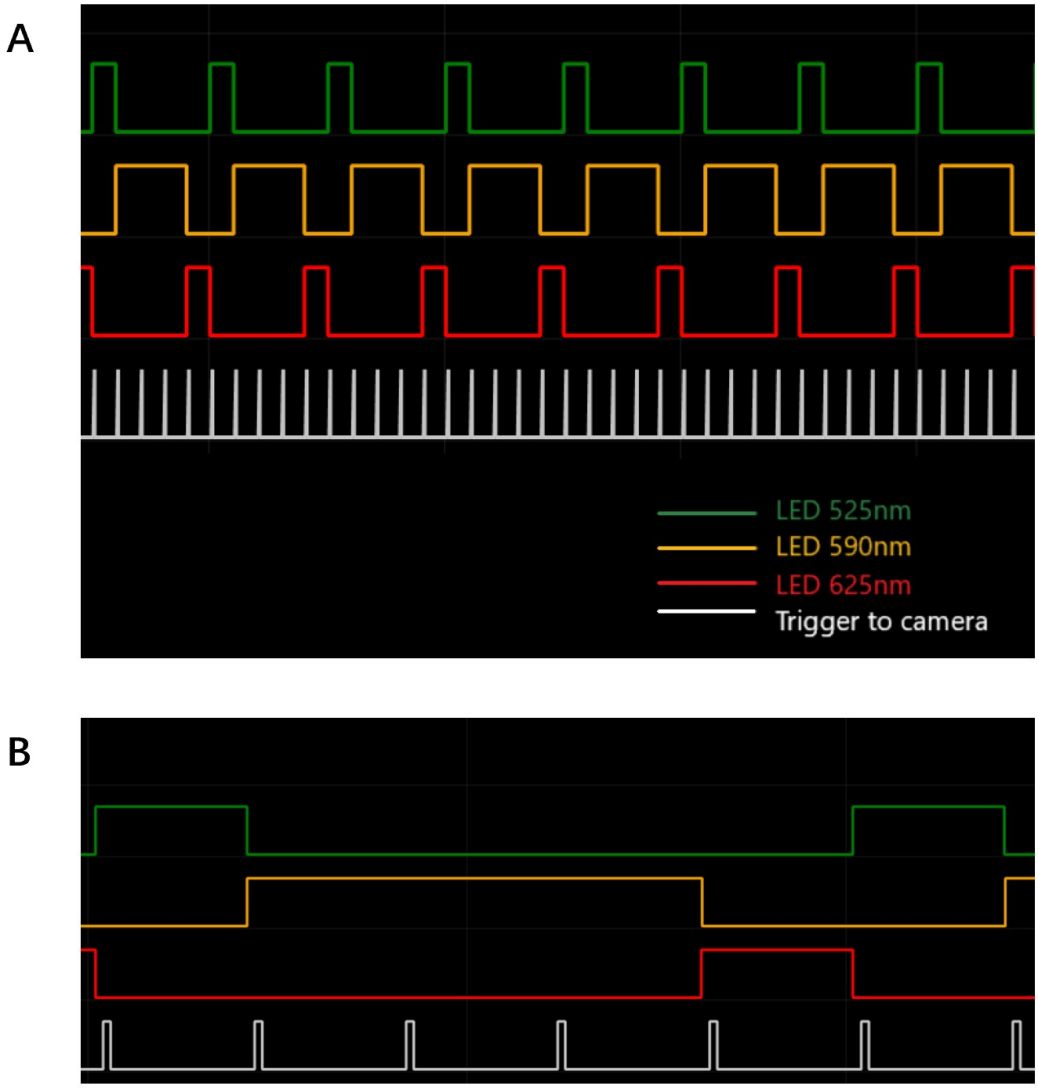

Figure 3·2: A This protocol is showing the sequence and duration for three LED channels and the time point of the camera triggering signal. **B**: We shined the 590nm light to mouse brain three times longer than the other two channels, and sent three triggering signals to the camera when the 590nm light was on in one cycle.

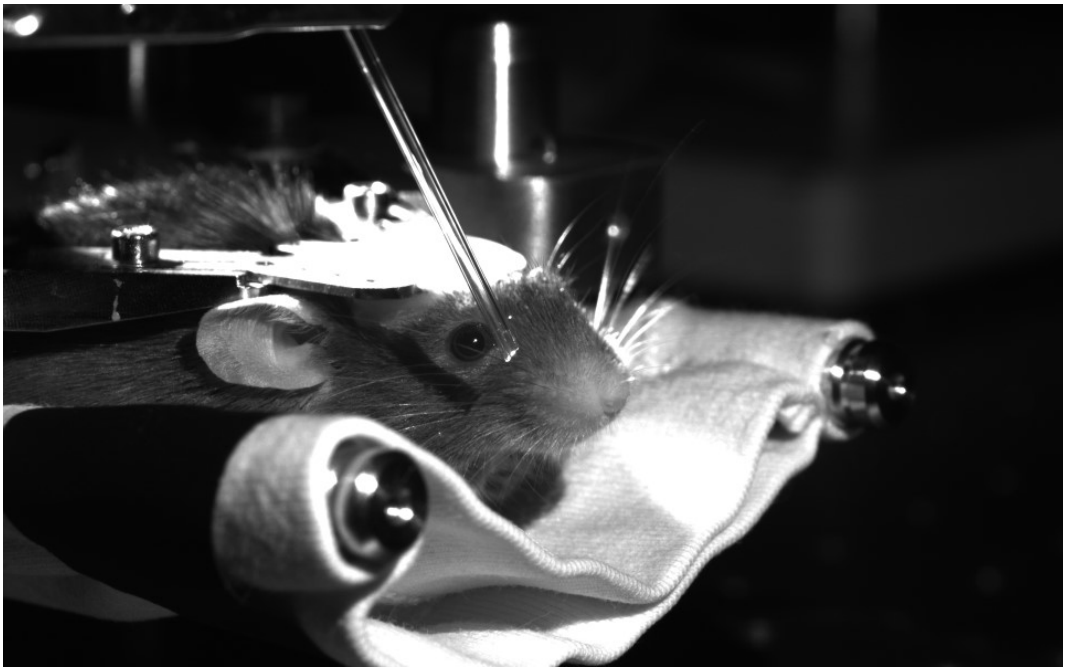

Figure 3·3: Picture acquired by the CCD camera was used to monitor mouse face.

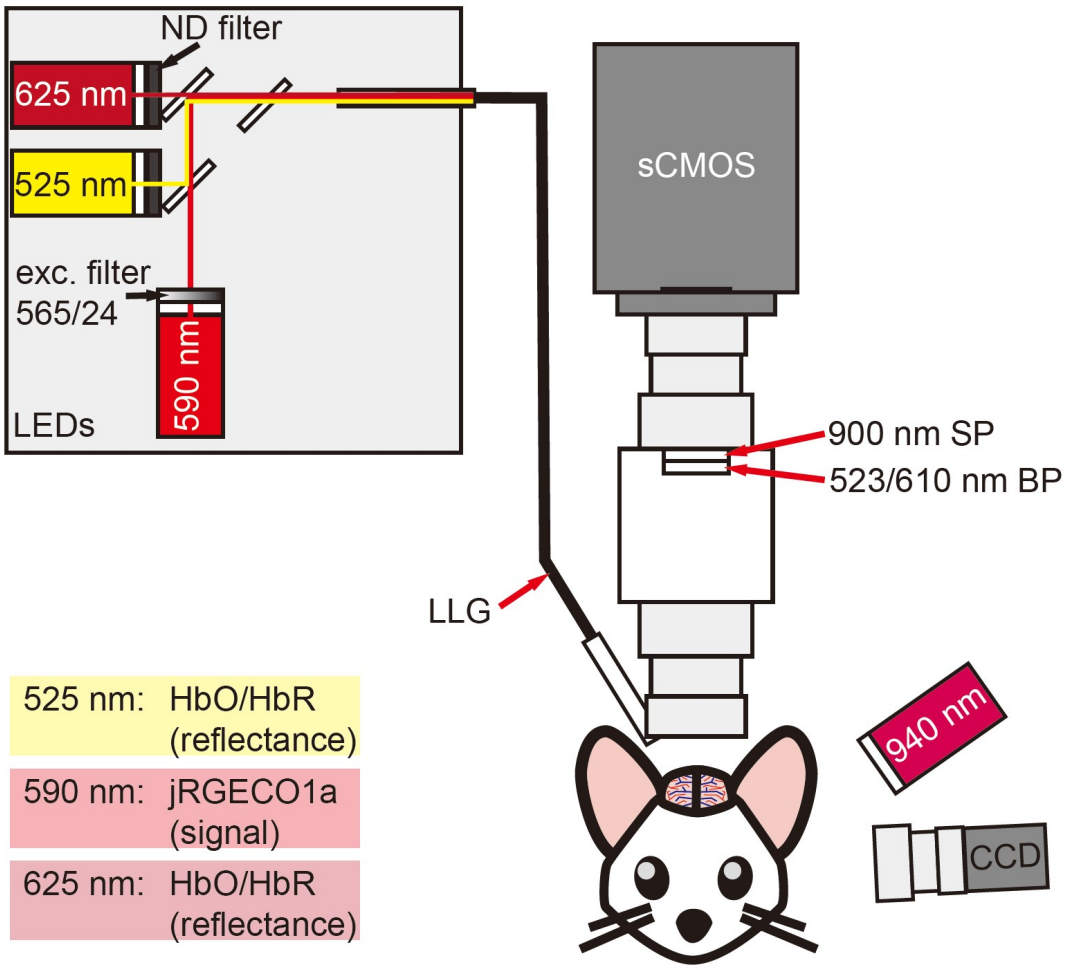

Figure 3·4: Mesoscopic imaging set up. LED source (Chrolis) served as the light source. The 525nm, 590nm, and 625nm channels were used. A 565nm/70nm filter was put at the initial point of the 590nm light path to select 570nm light, which meets the highest efficiency of jRGECO excitation. Lights from three channels were shined to the cranial window sequentially following a custom protocol. Mouse face were monitored by a CCD camera, and a 940nm LED light was used to illuminate the mouse face. The images of the brain were collected by a sCOMS camera. 900nm short-pass filter and 523/610nm bandpass filter were used to select the light that could go through the camera.

3.4 Microscopic imaging setup

To observe the vessel leakage introduced by repeated FUS-BBB opening treatments, we injected fluorescein isothiocyanate (FITC)-labeled dextran into the mouse tail vein right after the first and third FUS-BBB opening treatments, which is usually blocked by the undisrupted blood brain barrier. Then we observed the vessel leakage using two-photon microscopy. We also retro-orbitally injected Alexa 680 dextran a week before the first treatment and after the fourth treatment. With air puff stimulation (3Hz, 2Sec, 15times), we measured the neuronal activity and vessel dilation using two-photon microscopy.

Images were obtained using an Ultima two-photon laser scanning microscopy system (Bruker Fluorescence Microscopy). Two-photon excitation was provided by a Chameleon Ultra femtosecond Ti:Sapphire laser (Coherent) tuned to 940 nm to excite FITC- dextran. For jRGECO1a and Alexa-680 dextran measurements, the laser emitted 800 nm into an Optical Parametric Oscillator (OPO). The OPO gave as output 1040 nm, which we used to excite jRGECO1a and Alexa-680 dextran.

We used a combination of Zeiss 5x objective (Plan-NEOFLUAR, NA=0.16) for a coarse imaging and Olympus 20x (UMPlanFI, NA=0.5) objective for fine navigation under the glass window and for two-photon imaging. The emission of jRGECO1a and Alexa-680 Dextran was reflected with a low-pass dichroic mirror (560-nm cut-off wavelength; custom-made by Chroma Technologies). jRGECO1a emission was subsequently filtered with a 617/70 nm emission filter, and the emission of Alexa-680 Dextran emission was filtered with a 736/128 nm emission filter. Both emissions were detected using a photomultiplier tube (PMT).

For experiments where we checked for leakage of FITC dextran after FUS treatment, we used a 525/70 emission filter. The mesoscopic imaging process diagram is shown in **Figure. 3.5**.

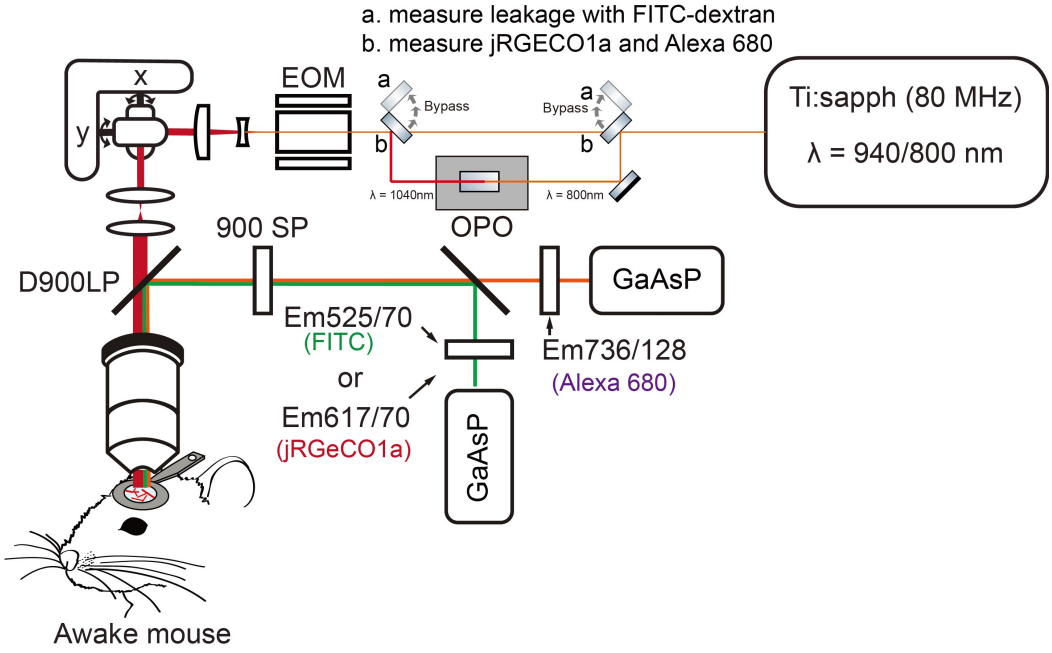

Figure 3·5: Two-photon imaging setup. 800nm or 940nm wavelength laser were generated by a Chameleon Ultra femtosecond Ti:Sapphire laser (Coherent). 940nm laser was used to excite FITX dextran. The emission light of FITC dextran was filtered with 525nm/70nm emission filter. 800nm laser went through OPO, The OPO gave 1040nm laser as output. 1040nm laser excited jRGECO and Anlexa 680 dextran at the same time. The jRGECO emission light was filtered with 617nm/70nm emission filter, and the Alexa 680 dextran emission light was filtered with 736nm/128nm emission filter. All emissions were detected by PMT.

3.5 Hemodynamic response function

Linear coupling between neuronal activity and the hemodynamic response was found in awake animals (Martin et al., 2006). To evaluate the alteration of neurovascular coupling, a least-squares deconvolution model (Ma et al., 2016) was used to calculate the hemodynamic response function (HRF) **(eq. 3.1)**.

$$y = X * h \tag{3.1}$$

where X is the input (ΔF/F), which is representing calcium signal; y is the output (Δ[HbT]), which is the hemodynamic signal; h is the convolution kernel, which is HRF in the context of neurovascular coupling. To avoid rank deficiency, we used a diagonal loading least-square deconvolution method. The weighted cost function for our model was **(eq. 3.2)**:

$$J(x) = ||y - Xh||_2^2 + \lambda\,||h||_2^2 \tag{3.2}$$

where J is the cost function, and λ is the constant weight. By minimizing the cost function (setting the derivative of the cost function to zero), the solution was given by the following:

$$h = (X^T X + \lambda I)^{(-1)} X^T y \tag{3.3}$$

where I is diagonal matrix. λ was defined as 0.1 in our calculation.

Chapter 4

Lmitations and Solutions

4.1 Allergic reactions to human albumin

The results of our study showed the suppression of neuronal activity and neurovascular uncoupling after the first and the third treatments. Besides the BBB disruption introduced by the focused ultrasound treatments, the microbubbles (Optison) we used in this study might also cause mice allergic reactions. Optison microbubble has been used to facilitate focused ultrasound to open the BBB in different studies (McDannold et al., 2007; Vykhodtseva et al., 2016). Therefore, we chose the Optison in this study to serve as the ultrasound contrast agent. However, mice died successively. At the beginning of our experiments, four mice were used, but only one mouse survived till the end of the fourth treatment week **(Figure.4.1)**. We chose Definity microbubbles instead for the further experiments. We have observed that the BBB opening occurred after focused ultrasound treatments facilitated by Definity microbubbles Trypan blue autofluorescence **(Figure. 2.8)**. We will continue the study with more experiments in the Summer of 2022.

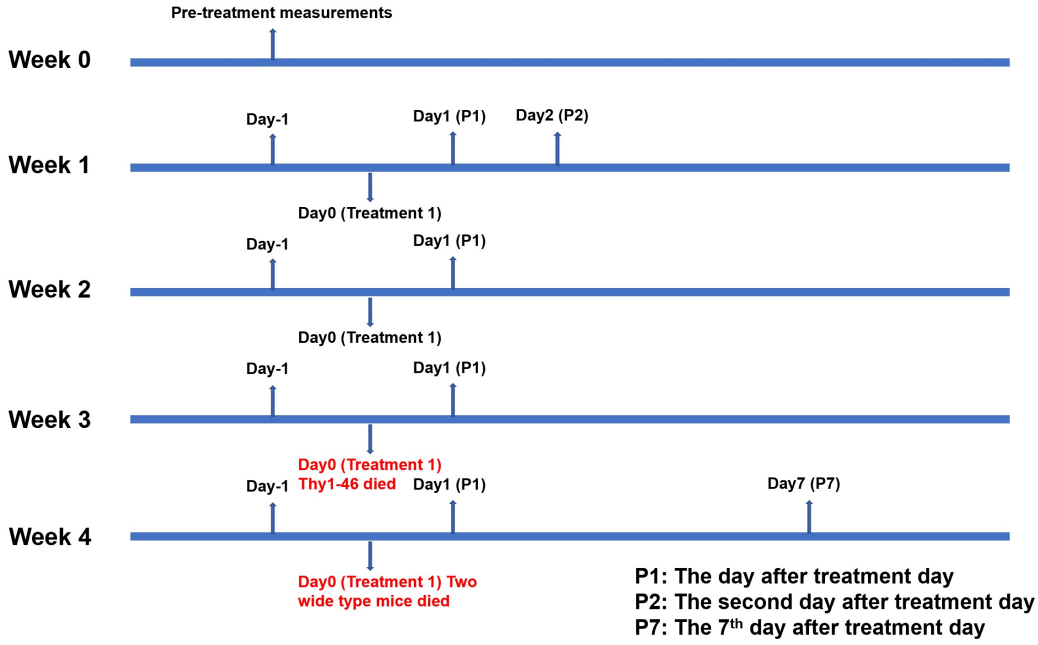

Figure 4·1: Three of four mice died in experiments. Mouse Thy1-46 died at the third treatments day, and two wide type mice died at the fourth treatments day.

4.2 Possible hemodynamic artifact

In this study, we evaluated the alteration of neurovascular coupling introduced by repeated focused ultrasound treatments. We used two-photon imaging to observe vessel leakage, vessel dilation, and neuronal activity. We also used mesoscopic imaging to capture the hemodynamic and neuronal activities simultaneously.

During mesoscopic imaging, the excitation and emission lights go through the tissue, including vessels, before or after interacting with the fluorophore related to neural activity. This phenomenon would have minimal consequences if the absorption properties along the light path were constant. However, based on the mechanism of neurovascular coupling, neural activity is always accompanied by hyperemia, resulting in the variation of absorption properties in the light path. Therefore, hemodynamic artifact correction strategies such as linear regression between neuronal activity de-

pendent and independent data are usually a part of calcium signal analysis (Ma et al., 2016). But in this study, the red-shifted calcium indicator jRGECO1a was used. The emission wavelength of jRGECO1a is around 600nm (Dana et al., 2018), while the absorption coefficients of hemoglobin drop off rapidly with the increasing wavelength around 590nm (Svoboda et al., 1994). Hemodynamic artifact correction on the data collected with red-shifted calcium indicator has shown a negligible difference with the uncorrected data (Lohani et al., 2021). Therefore, we didn't apply hemodynamic artifact correction to our current data. To evaluate the need of hemodynamic correction, we will do control experiments with mApple, which should not change in response to neuronal activity.

4.3 Off-peak excitation

The peak of jRGECO1a excitation light used in mesoscopic imaging was off the peak of jRGECO1a excitation spectra, which was another limitation of this study. Although we summed up the images collected multiple times corresponding to neuronal activity, we still got low fluorescence intensities, which reduced the SNR of our data. To enhance the SNR of our images, we replaced the excitation light source to match the excitation peak of jRGECO1a excitation spectra. In the experiments in summer, we will collect images with higher SNR.

Chapter 5

Conclusion

Focused ultrasound treatments have been clinically applied in a broad range of therapies, including cerebral tumor treatment (Toccaceli et al., 2019), Alzheimer's diseases treatment (Lipsman et al., 2018), and amyotrophic lateral sclerosis (ALS) treatments (Abrahao et al., 2019). Safe parameters have been investigated by most early research, while the secondary effects are still uncleared. Our study provided an initial step to evaluate the disruption of neurovascular coupling introduced by focused ultrasound treatments. In our experiments, negligible alteration in neurovascular coupling has been observed. With three major limitations, we collected insufficient data. In the future, we will continue this study with Definity microbubbles, and provide an understanding of the secondary effects of the focused ultrasound treatments.

References

Abbott, N. J., Patabendige, A. A. K., Dolman, D. E. M., Yusof, S. R., and Begley, D. J. (2010). Structure and function of the blood–brain barrier. *Neurobiology of Disease*, 37(1):13–25.

Abrahao, A., Meng, Y., Llinas, M., Huang, Y., Hamani, C., Mainprize, T., Aubert, I., Heyn, C., Black, S. E., Hynynen, K., Lipsman, N., and Zinman, L. (2019). First-in-human trial of blood–brain barrier opening in amyotrophic lateral sclerosis using MR-guided focused ultrasound. *Nature Communications*, 10(1):4373.

Allen, W. E., Kauvar, I. V., Chen, M. Z., Richman, E. B., Yang, S. J., Chan, K., Gradinaru, V., Deverman, B. E., Luo, L., and Deisseroth, K. (2017). Global Representations of Goal-Directed Behavior in Distinct Cell Types of Mouse Neocortex. *Neuron*, 94(4):891–907.e6.

Aryal, M., Arvanitis, C. D., Alexander, P. M., and McDannold, N. (2014). Ultrasound-mediated blood–brain barrier disruption for targeted drug delivery in the central nervous system. *Advanced Drug Delivery Reviews*, 72:94–109.

Chatterjee, S. and Fisher, A. B. (2014). Mechanotransduction in the Endothelium: Role of Membrane Proteins and Reactive Oxygen Species in Sensing, Transduction, and Transmission of the Signal with Altered Blood Flow. *Antioxidants & Redox Signaling*, 20(6):899–913.

Chen, G., Saad, Z. S., Adleman, N. E., Leibenluft, E., and Cox, R. W. (2015). Detecting the subtle shape differences in hemodynamic responses at the group level. *Frontiers in Neuroscience*, 9.

Chen, S., Nazeri, A., Baek, H., Ye, D., Yang, Y., Yuan, J., Rubin, J. B., and Chen, H. (2022). A review of bioeffects induced by focused ultrasound combined with microbubbles on the neurovascular unit. *Journal of Cerebral Blood Flow & Metabolism*, 42(1):3–26.

Dana, H., Novak, O., Guardado-Montesino, M., Fransen, J. W., Hu, A., Borghuis, B. G., Guo, C., Kim, D. S., and Svoboda, K. (2018). Thy1 transgenic mice expressing the red fluorescent calcium indicator jRGECO1a for neuronal population imaging in vivo. *PLOS ONE*, 13(10):e0205444.

Daneman, R. and Prat, A. (2015). The Blood–Brain Barrier. *Cold Spring Harbor Perspectives in Biology*, 7(1):a020412.

Girouard, H. and Iadecola, C. (2006). Neurovascular coupling in the normal brain and in hypertension, stroke, and Alzheimer disease. *Journal of Applied Physiology*, 100(1):328–335.

Gross, P. M., Wall, K. M., Pang, J. J., Shaver, S. W., and Wainman, D. S. (1990). Microvascular specializations promoting rapid interstitial solute dispersion in nucleus tractus solitarius. *American Journal of Physiology-Regulatory, Integrative and Comparative Physiology*, 259(6):R1131–R1138.

Hendrikx, D., Smits, A., Lavanga, M., De Wel, O., Thewissen, L., Jansen, K., Caicedo, A., Van Huffel, S., and Naulaers, G. (2019). Measurement of Neurovascular Coupling in Neonates. *Frontiers in Physiology*, 10.

Hersh, D. S., Wadajkar, A. S., Roberts, N., Perez, J. G., Connolly, N. P., Frenkel, V., Winkles, J. A., Woodworth, G. F., and Kim, A. J. (2016). Evolving Drug Delivery Strategies to Overcome the Blood Brain Barrier. *Current pharmaceutical design*, 22(9):1177–1193.

Hynynen, K., McDannold, N., Sheikov, N. A., Jolesz, F. A., and Vykhodtseva, N. (2005). Local and reversible blood–brain barrier disruption by noninvasive focused ultrasound at frequencies suitable for trans-skull sonications. *NeuroImage*, 24(1):12–20.

Hynynen, K., McDannold, N., Vykhodtseva, N., and Jolesz, F. A. (2001). Noninvasive MR Imaging–guided Focal Opening of the Blood-Brain Barrier in Rabbits. *Radiology*, 220(3):640–646.

Iadecola, C. (2017). The Neurovascular Unit Coming of Age: A Journey through Neurovascular Coupling in Health and Disease. *Neuron*, 96(1):17–42.

Jordão, J. F., Ayala-Grosso, C. A., Markham, K., Huang, Y., Chopra, R., McLaurin, J., Hynynen, K., and Aubert, I. (2010). Antibodies Targeted to the Brain with Image-Guided Focused Ultrasound Reduces Amyloid-β Plaque Load in the TgCRND8 Mouse Model of Alzheimer's Disease. *PLOS ONE*, 5(5):e10549.

Kisler, K., Nelson, A. R., Montagne, A., and Zlokovic, B. V. (2017). Cerebral blood flow regulation and neurovascular dysfunction in Alzheimer disease. *Nature Reviews Neuroscience*, 18(7):419–434.

Kleinfeld, D., Blinder, P., Drew, P., Driscoll, J., Muller, A., Tsai, P., and Shih, A. (2011). A Guide to Delineate the Logic of Neurovascular Signaling in the Brain. *Frontiers in Neuroenergetics*, 3.

Kovacs, Z. I., Burks, S. R., and Frank, J. A. (2018). Focused ultrasound with microbubbles induces sterile inflammatory response proportional to the blood brain barrier opening: Attention to experimental conditions. *Theranostics*, 8(8):2245–2248.

Kovacs, Z. I., Kim, S., Jikaria, N., Qureshi, F., Milo, B., Lewis, B. K., Bresler, M., Burks, S. R., and Frank, J. A. (2017). Disrupting the blood-brain barrier by focused ultrasound induces sterile inflammation. *Proceedings of the National Academy of Sciences of the United States of America*, 114(1):E75–E84.

Lecrux, C. and Hamel, E. (2011). The neurovascular unit in brain function and disease. *Acta Physiologica*, 203(1):47–59.

Lipsman, N., Meng, Y., Bethune, A. J., Huang, Y., Lam, B., Masellis, M., Herrmann, N., Heyn, C., Aubert, I., Boutet, A., Smith, G. S., Hynynen, K., and Black, S. E. (2018). Blood–brain barrier opening in Alzheimer's disease using MR-guided focused ultrasound. *Nature Communications*, 9(1):2336.

Lohani, S., Moberly, A. H., Benisty, H., Landa, B., Jing, M., Li, Y., Higley, M. J., and Cardin, J. A. (2021). Dual color mesoscopic imaging reveals spatiotemporally heterogeneous coordination of cholinergic and neocortical activity. *BioRxiv*. https://doi.org/10.1101/2020.12.09.418632.

Ma, Y., Shaik, M. A., Kim, S. H., Kozberg, M. G., Thibodeaux, D. N., Zhao, H. T., Yu, H., and Hillman, E. M. C. (2016a). Wide-field optical mapping of neural activity and brain haemodynamics: Considerations and novel approaches. *Philosophical Transactions of the Royal Society B: Biological Sciences*, 371(1705):20150360.

Ma, Y., Shaik, M. A., Kozberg, M. G., Kim, S. H., Portes, J. P., Timerman, D., and Hillman, E. M. C. (2016b). Resting-state hemodynamics are spatiotemporally coupled to synchronized and symmetric neural activity in excitatory neurons. *Proceedings of the National Academy of Sciences*, 113(52):E8463–E8471.

Martin, C., Martindale, J., Berwick, J., and Mayhew, J. (2006). Investigating neural–hemodynamic coupling and the hemodynamic response function in the awake rat. *NeuroImage*, 32(1):33–48.

McDannold, N., Vykhodtseva, N., and Hynynen, K. (2008). Effects of Acoustic Parameters and Ultrasound Contrast Agent Dose on Focused-Ultrasound Induced Blood-Brain Barrier Disruption. *Ultrasound in Medicine & Biology*, 34(6):930–937.

McMahon, D., Bendayan, R., and Hynynen, K. (2017). Acute effects of focused ultrasound-induced increases in blood-brain barrier permeability on rat microvascular transcriptome. *Scientific Reports*, 7(1):45657.

McMahon, D. and Hynynen, K. (2017). Acute Inflammatory Response Following Increased Blood-Brain Barrier Permeability Induced by Focused Ultrasound is Dependent on Microbubble Dose. *Theranostics*, 7(16):3989–4000.

Meairs, S. (2015). Facilitation of Drug Transport across the Blood–Brain Barrier with Ultrasound and Microbubbles. *Pharmaceutics*, 7(3):275–293.

Metea, M. R. and Newman, E. A. (2006). Glial Cells Dilate and Constrict Blood Vessels: A Mechanism of Neurovascular Coupling. *Journal of Neuroscience*, 26(11):2862–2870.

Muoio, V., Persson, P. B., and Sendeski, M. M. (2014). The neurovascular unit – concept review. *Acta Physiologica*, 210(4):790–798.

Nicholas, A. P. and Whitaker, J. N. (2002). Preparation of a monoclonal antibody to citrullinated epitopes: Its characterization and some applications to immunohistochemistry in human brain. *Glia*, 37(4):328–336.

Pardridge, W. M. (2005). The Blood-Brain Barrier: Bottleneck in Brain Drug Development. *NeuroRX*, 2(1):3–14.

Park, E.-J., Zhang, Y.-Z., Vykhodtseva, N., and McDannold, N. (2010). Enhanced permeability of tumor blood vessels in brain using focused ultrasound with microbubbles. In *2010 IEEE International Ultrasonics Symposium*, pages 2123–2126.

Rangaprakash, D., Tadayonnejad, R., Deshpande, G., O'Neill, J., and Feusner, J. D. (2021). FMRI hemodynamic response function (HRF) as a novel marker of brain function: Applications for understanding obsessive-compulsive disorder pathology and treatment response. *Brain Imaging and Behavior*, 15(3):1622–1640.

Raymond, S. B., Skoch, J., Hynynen, K., and Bacskai, B. J. (2007). Multiphoton Imaging of Ultrasound/Optison Mediated Cerebrovascular Effects in vivo. *Journal of Cerebral Blood Flow & Metabolism*, 27(2):393–403.

Raymond, S. B., Treat, L. H., Dewey, J. D., McDannold, N. J., Hynynen, K., and Bacskai, B. J. (2008). Ultrasound Enhanced Delivery of Molecular Imaging and Therapeutic Agents in Alzheimer's Disease Mouse Models. *PLOS ONE*, 3(5):e2175.

Sheikov, N., McDannold, N., Vykhodtseva, N., Jolesz, F., and Hynynen, K. (2004). Cellular mechanisms of the blood-brain barrier opening induced by ultrasound in presence of microbubbles. *Ultrasound in Medicine & Biology*, 30(7):979–989.

Siesjö, B. K. and Plum, F. (1971). Cerebral Energy Metabolism in Normoxia and in Hypoxia. *Acta Anaesthesiologica Scandinavica*, 15(s45):81–101.

Sinharay, S., Tu, T.-W., Kovacs, Z. I., Schreiber-Stainthorp, W., Sundby, M., Zhang, X., Papadakis, G. Z., Reid, W. C., Frank, J. A., and Hammoud, D. A. (2019). In vivo imaging of sterile microglial activation in rat brain after disrupting the blood-brain barrier with pulsed focused ultrasound: [18F]DPA-714 PET study. *Journal of Neuroinflammation*, 16(1):155.

Svoboda, K. and Block, S. M. (1994). Biological Applications of Optical Forces. *Annual Review of Biophysics and Biomolecular Structure*, 23(1):247–285.

Toccaceli, G., Barbagallo, G., and Peschillo, S. (2019). Low-intensity focused ultrasound for the treatment of brain diseases: Safety and feasibility. *Theranostics*, 9(2):537–539.

Todd, N., Angolano, C., Ferran, C., Devor, A., Borsook, D., and McDannold, N. (2020). Secondary effects on brain physiology caused by focused ultrasound-mediated disruption of the blood–brain barrier. *Journal of Controlled Release*, 324:450–459.

Todd, N., Zhang, Y., Livingstone, M., Borsook, D., and McDannold, N. (2019). The neurovascular response is attenuated by focused ultrasound-mediated disruption of the blood-brain barrier. *NeuroImage*, 201:116010.

Tsai, M.-T., Lee, C.-K., Lin, K.-M., Lin, Y.-X., Lin, T.-H., Chang, T.-C., Lee, J.-D., and Liu, H.-L. (2013). Quantitative observation of focused-ultrasound-induced vascular leakage and deformation via fluorescein angiography and optical coherence tomography. *Journal of Biomedical Optics*, 18(10):101307.

Valley, M. T., Moore, M. G., Zhuang, J., Mesa, N., Castelli, D., Sullivan, D., Reimers, M., and Waters, J. (2020). Separation of hemodynamic signals from GCaMP fluorescence measured with wide-field imaging. *Journal of Neurophysiology*, 123(1):356–366.

Vykhodtseva, N., McDannold, N., and Hynynen, K. (2006). Induction of apoptosis in vivo in the rabbit brain with focused ultrasound and Optison®. *Ultrasound in Medicine & Biology*, 32(12):1923–1929.

Wekselblatt, J. B., Flister, E. D., Piscopo, D. M., and Niell, C. M. (2016). Large-scale imaging of cortical dynamics during sensory perception and behavior. *Journal of Neurophysiology*, 115(6):2852–2866.

Wu, S.-K., Tsai, C.-L., Huang, Y., and Hynynen, K. (2021). Focused Ultrasound and Microbubbles-Mediated Drug Delivery to Brain Tumor. *Pharmaceutics*, 13(1):15.

CURRICULUM VITAE